Amirkabir Univ. of Technology
Aerospace Engineering Dept.

The Third Fuel & Combustion Conference of IRAN

Tehran - IRAN Feb. 2010

Iranian Combustion Institue

FCCI2010-1148

TWO DIMENSIONAL STUDY OF METHANE AUTOTHERMAL REFORMING IN A CATALYTIC SURFACE MICRO-REACTOR

M.H. Akbari[*,§], M. Andisheh Tadbir[**], A.H. Sharafian Ardakani[**]
[*] Assistant professor, Faculty of Mechanical Engineering, Shiraz University, Shiraz, Iran
[**] M.Sc. student, Faculty of Mechanical Engineering, Shiraz University, Shiraz, Iran

([§] Correspondent author's E-mail: h-akbari@shirazu.ac.ir)

ABSTRACT Autothermal reforming (ATR) of hydrocarbons, such as methane, is an interesting method for hydrogen production mainly because of its neutral thermal behavior. It is particularly suitable for mobile applications considering its response time and volume characteristics. In this investigation, a two dimensional catalytic ATR micro-reactor is simulated numerically. The governing equations for the flow field and chemical species are solved using an in-house CFD code. A four-reaction mechanism is implemented to model the reactions that occur on the wall surfaces of the micro-reactor in the presence of Ni/Al_2O_3 catalyst. The effects of some parameters on the methane conversion and hydrogen yield are studied. These parameters include the reactor length and width, and the inlet flow rate. Results from these simulations indicate that at a relative reactor length (L/D) of 60, methane conversion is 78.2% and the hydrogen yield is 50%. It is also observed that as the reactor width is increased from 100 μm to 400 μm, for a fixed reactor length, methane conversion will decrease from 61% to 56% and hydrogen yield changes from 46.4% to 39.5%. Simulation results also indicate that at a volumetric flow rate of 25 mm^2/s, the hydrogen yield reaches a maximum value while the methane conversion is 63.6%. Considering these results, the optimum dimensions of the channel and gas hourly space velocity are determined for the highest hydrogen yield.

Keywords autothermal reforming; hydrogen production; micro-reactor; surface reaction.

INTRODUCTION

Growth of energy consumption in recent decades has become a major issue partly because of its environmental impact and partly due to the limited available energy resources. Underground fossil fuels will approximately end in 40 years, therefore finding other sources of energy is inevitable. Hydrogen is considered as the most suitable energy carrier in the future because of its compatibility with the new energy sources and its little environmental impact. In the meantime, commercial production of hydrogen in a compact reactor, which is suitable for mobile applications, is of great interest [Ahmed S. 2001, Biesheuvel P.M. 2003].
Hydrogen can be used as the main fuel in all types of fuel cell, but the costs for its delivery and storage is very high at the present. In addition, hydrogen energy density is very low and hence hydrogen storage is not considered practical for many applications. If hydrogen can be produced on-demand, the problems regarding its storage or delivery will be eliminated. Three major thermo-chemical reforming techniques are available to produce hydrogen from other

hydrocarbon fuels; these include steam reforming (SR), partial oxidation (POX), and autothermal reforming (ATR).

SR is a conventional method of hydrogen production in some industries but it is extremely endothermic and the reformer needs external heat for its operation. Thus, the resulting configuration for the reactor becomes heavy and bulky, which is not suitable for a portable fuel cell system.

POX is another method for hydrogen production, which is exothermic with easy start up even in the absence of a catalyst. Hence, the problems stated earlier regarding SR will no longer exist. But there is another problem; the CO concentration produced by this method is too high for a PEM fuel cell and further treatments of the synthesis gas will be needed.

ATR is the technique with fewer problems compared with others. To produce hydrogen by this method, fuel, water and air are fed into the reactor. The presence of water and air will result in simultaneous occurrence of SR and POX reactions at the presence of a catalyst in the reactor. The endothermic nature of SR and exothermic nature of POX make the overall reaction thermally neutral. In other words, the heat release from the POX reaction will supply the heat required by the SR reaction. Consequently, the overall temperature will be lowered (compared to POX) which is favourable to the water-gas shift (WGS) reaction, in which the generated carbon-monoxide by POX will convert into carbon-dioxide and hydrogen. The aforementioned advantages have encouraged researchers to work on different aspects of ATR for hydrogen production, particularly for portable devices [Heinzel A. 2002, Armor JN. 2005].

Trimm and Lam [1980] were among the first who studied ATR of methane. They measure ATR reaction kinetics on Pt/Al_2O_3 fibre catalyst at temperatures around 800 K. Xu and Froment [1989] developed intrinsic kinetic for methane steam reforming, methanation, and water-gas shift reactions on Ni/Al_2O_3 catalyst for initial temperature rang among 573–823 K. This mechanism has been implemented in numerous investigations up to now.

Ma *et al.* [1996] designed and tested an autothermal reactor for the conversion of light hydrocarbon to hydrogen on $Pt/\delta\text{-}Al_2O_3$ catalyst. They presented a kinetic rate equation for the reaction of methane total combustion based on this catalyst for initial temperature rang of 663–723 K.

Groote and Froment [1996] simulated the catalytic POX of methane to synthesis gas on a Ni catalyst in an adiabatic reactor with various inlet molar air to fuel (A/F) and molar water to fuel (W/F) ratios. The kinetic rates were presented for eight reactions and a series of effectiveness factors associated with these reactions were proposed.

Shukri *et al.* [2004] modelled a one-dimensional steady state adiabatic fixed bed reactor. In this study, effects of operating pressure, inlet temperature and steam to methane ratio were investigated. They showed that increase of steam to methane ratio over a certain value would decrease the methane conversion.

Halabi *et al.* [2008] modelled and analyzed a one-dimensional heterogeneous autothermal reactor of methane to hydrogen with gas feed temperature and pressure of 773 K and 1.5 bar in a Ni/Al_2O_3 fixed-bed reformer. The influence of different parameters such as oxygen/carbon and steam/carbon were investigated. The optimum conditions were located in a space velocity (SV) range from 1,050 to 14,000 h^{-1}, steam/carbon molar ratio of 4.5–6.5 and oxygen/carbon molar ratio of 0.45–0.55 to obtain maximum conversion of hydrogen.

Most of the previous investigations were carried out for packed-bed reactors (with volumetric reactions). In the present study, catalytic ATR of methane in a surface microreactor at the

presence of a Ni based catalyst is numerically simulated. A two-dimensional, steady-state, adiabatic model is developed. In the present study, the effects of some parameters on the methane conversion and hydrogen yield are studied. These parameters include the reactor dimensions and the inlet flow rate.

NUMERICAL SIMULATION

Model Assumptions The flow regime is assumed to be steady, incompressible and laminar. The gas mixture is treated as an ideal gas with variable properties based on the local composition. The gas flow mixture consists of 7 species: CH_4, O_2, CO, CO_2, H_2, H_2O and N_2. Furthermore, Dufour and Soret effects are neglected in the species mass diffusion.

Governing Equations Governing equations include conservations of mass, momentum, energy and chemical species, as well as the ideal gas mixture equation.
The continuity equation for a steady-state flow in a Cartesian coordinate is given by Eq. 1.

$$\nabla.\left(\rho\vec{V}\right)=0 \tag{1}$$

The conservation of momentum is stated by the Navier-Stokes equation, given below.

$$\vec{V}.\nabla\left(\rho\vec{V}\right)=-\nabla p+\nabla\cdot\left(\mu\nabla\vec{V}\right) \tag{2}$$

Chemical species conservation for the i^{th} species is given by Eq. 3, with the molar production rate given by Eq. 4.

$$\nabla.\left(\rho\vec{V}\,Y_i\right)=\nabla.\left(D_{eff,i}\rho\nabla Y_i\right)+\omega_i MW_i \tag{3}$$

$$\omega_i=\rho_{cat}\sum_{j=1}^{4}\left(\xi_{ij}\,R_j\,\eta_j\right) \tag{4}$$

Nitrogen does not participate in any reaction, therefore, Eqs. 3 and 4 are applied only for 6 species. Nitrogen mass fraction is obtained from Eq. 5.

$$Y_{N_2}=1-\sum_{i,i\neq N_2}Y_i \tag{5}$$

It is necessary to note that the source term, $\omega_i MW_i$, in Eq. 3 is zero for the internal cells of the computational domain, because reactions occur only on the walls.
Conservation of energy is implemented to calculate the temperature, as given by Eq. 6.

$$\nabla.\left(\rho c_p\vec{V}\,T\right)=\nabla.\left(k\nabla T\right)+\rho_{cat}\sum_{i=1}^{4}\left(\Delta H_i\,R_i\,\eta_i\right) \tag{6}$$

For the same reason given above, the source term in this equation is non-zero only on the internal walls of the reactor.
Gas mixture density is computed using the ideal gas relationship for a multi-component mixture which is given in Eq. 7. However, since the temperature and pressure have negligible variations along the simulated ATR microreactor, the temperature and pressure are taken at their inlet values in the following equation.

$$\rho=\frac{P\,MW_{mix}}{R_u T} \tag{7}$$

The mixture molecular weight in the above equation is computed from the following.

$$MW_{mix} = \sum_i \chi_i MW_i = \frac{1}{\sum_i \frac{Y_i}{MW_i}} \tag{8}$$

The effective mass diffusion coefficient, D_{eff}, in Eq. 3 is computed using Eq. 9.

$$D_{eff,i} = \frac{1-\chi_i}{\sum_{j\neq i}^{\forall j} \frac{\chi_j}{D_{ij}}} \tag{9}$$

In this equation D_{ij} is the binary diffusion coefficient. The binary mass diffusivity is calculated by the relationships given by Reid *et al.* [1987]. The methodology is based on the Chapman-Enskog theoretical description of a binary mixture of gases at low to moderate pressures. In this theory, the binary diffusion coefficient for the species pair i and j is given by Eqs. 10-14.

$$D_{ij} = \frac{0.0266\,T^{3/2}}{P\,MW_{ij}^{1/2}\,\sigma_{ij}^2\,\Omega_D} \tag{10}$$

$$MW_{ij} = 2\left[\left(1/MW_i\right)+\left(1/MW_j\right)\right]^{-1} \tag{11}$$

$$\sigma_{ij} = \left(\sigma_i+\sigma_j\right)/2 \tag{12}$$

$$\Omega_D = \frac{1.06036}{\left(T^*\right)^{0.15610}} + \frac{0.19300}{\exp\left(0.47635\,T^*\right)} + \frac{1.03587}{\exp\left(1.52996\,T^*\right)} + \frac{1.76474}{\exp\left(3.89411\,T^*\right)} \tag{13}$$

$$T^* = k_B T/\left(\varepsilon_i\,\varepsilon_j\right)^{1/2} \tag{14}$$

Table 1 gives the values of hard-sphere collision diameter, σ, as well as Lennard-Jones energy, ε, for various species involved in our calculations.

Table 1
Hard–sphere collision diameter and Lennard–Jones energy parameter for each species

Species	$\sigma\left(\mathring{\mathrm{A}}\right)$	$\varepsilon/k_B\ (K)$
CH_4	3.758	148.6
O_2	3.467	106.7
CO_2	3.941	195.2
H_2O	2.641	809.1
CO	3.690	91.7
H_2	2.827	59.7
N_2	3.798	71.4

The constant pressure specific heat, dynamic viscosity, and thermal conductivity of the gas mixture are computed using Eqs. 15-17.

$$c_{p,eff} = \sum_i c_{p,i} Y_i \tag{15}$$

$$\mu_{eff} = \sum_i \mu_i Y_i \tag{16}$$

$$k_{eff} = \sum_i k_i \chi_i \tag{17}$$

Methane conversion is given by the following equation.

$$CH_4\ conversion\ (\%) = \frac{\chi_{CH_4}^{in} - \chi_{CH_4}^{out}}{\chi_{CH_4}^{in}} \times 100 \tag{18}$$

Chemical Kinetics Most proposed mechanisms for ATR contain many reactions which make the numerical simulations complex and difficult to solve. Some of these reactions are reported by Halabi *et al.* [2008]. Excluding the non-significant reactions that posses low rates is a usual approach that makes the calculations practicable with reasonable accuracy. Therefore, as it has been shown [Hoang 2004, Halabi 2008] that four reactions can be considered as the major reactions which are listed below.

1) The exothermic total combustion of methane,

R1: $CH_4 + 2O_2 \rightarrow CO_2 + 2H_2O$, ΔH_{298} = -802 kJ/mol (19)

2) The endothermic steam reforming of methane to carbon monoxide,

R2: $CH_4 + H_2O \leftrightarrow CO + 3H_2$, ΔH_{298} = 206 kJ/mol (20)

3) The water-gas shift reaction,

R3: $CO + H_2O \leftrightarrow CO_2 + H_2$, ΔH_{298} = -41 kJ/mol (21)

4) The steam reforming of methane directly to carbon dioxide.

R4: $CH_4 + 2H_2O \leftrightarrow CO_2 + 4H_2$, ΔH_{298} = 165 kJ/mol (22)

An acceptable kinetic rate model for methane steam reforming over Ni-based catalyst was reported by Xu and Froment [1989]. Their suggested kinetic rate equation has been used extensively in different investigations. Two different kinetic rate equations are reported for the total methane combustion. One is reported by Trimm and Lam [1980] and the other is provided by Ma *et al.* [1996]. The former is for methane combustion over Pt-based catalyst at a fixed temperature, while the latter is based on the Langmuir-Hinshelwood model adjusted for Ni-based catalyst.

In the present study, SR and WGS reaction rates are computed using the model suggested in Xu and Froment [1989], and the reaction rate of methane combustion is obtained from Ma *et al.* [1986].

The corresponding kinetic rate equations for the above reactions are given in Eqs. 23-27.

$$R_1 = \frac{k_1 p_{CH_4} p_{O_2}^{1/2}}{(1 + K_{CH_4}^C p_{CH_4} + K_{O_2}^C p_{O_2}^{1/2})^2} \tag{23}$$

$$R_2 = \frac{k_2}{p_{H_2}^{2.5}} \left(p_{CH_4} p_{H_2O} - \frac{p_{H_2}^3 p_{CO}}{K_{e^2}} \right) \times \frac{1}{Q_r^2} \tag{24}$$

$$R_3 = \frac{k_3}{p_{H_2}}\left(p_{CO}p_{H_2O} - \frac{p_{H_2}p_{CO_2}}{K_{e^3}}\right)\times\frac{1}{Q_r^2} \tag{25}$$

$$R_4 = \frac{k_4}{p_{H_2}^{3.5}}\left(p_{CH_4}p_{H_2O}^2 - \frac{p_{H_2}^4 p_{CO_2}}{K_{e^4}}\right)\times\frac{1}{Q_r^2} \tag{26}$$

$$Q_r = 1 + K_{CO}p_{CO} + K_{H_2}p_{H_2} + K_{CH_4}p_{CH_4} + K_{H_2O}\frac{p_{H_2O}}{p_{H_2}} \tag{27}$$

In the above relations, $k_j = k_{oj}\times e^{(-E_j)/R_uT}$ is the kinetic rate constant of reaction j (j = reactions R1-R4), in which k_1 is determined from the data of Ma *et al.* [1986], while k_2 to k_4 are from Xu and Froment [1989]. k_{oj} and E_j are given in Table 2. K_{e^j} in Eqs. 24-26 is the equilibrium constant of reaction j (j = reactions R2-R4) which can be found in Table 3. $K_i^C = K_{oi}^C \times e^{(-\Delta H_C^i)/R_uT}$ in Eq. 23 is the adsorption constant of species i (i = CH_4, O_2) in the combustion reaction R1 and can be found in Table 4. Furthermore, $K_i = K_{oi}\times e^{(-\Delta H^i)/R_uT}$ in Eq. 27 is the adsorption constant of species i (i = CO, H_2, CH_4, H_2O) in the reforming reactions R2-R4 which can also be found in Table 4.

Table 2
Kinetic parameters

Reaction	k_{oj} (kmol/kg cat h)	E_j (kJ/kmol)
R1	5.852×10^{17} ($bar^{-1.5}$)	204,000
R2	4.225×10^{15} ($bar^{0.5}$)	240,100
R3	1.955×10^{6} ($bar^{-1.0}$)	67,130
R4	1.020×10^{15} ($bar^{0.5}$)	243,900

Table 3
Equilibrium constants

Reaction	Equilibrium constant K_{e^j}
R2	$5.75 \times 10^{12}\exp(-11476/T)$ (bar^2)
R3	$1.26 \times 10^{-2}\exp(4639/T)$
R4	$7.24 \times 10^{10}\exp(-21646/T)$ (bar^2)

The final equations for the calculation of the reaction rate for each species are summarized as follows:

$$\begin{aligned}
r_{CH4} &= -\eta_1 R_1 - \eta_2 R_2 - \eta_4 R_4 \\
r_{O2} &= -2\eta_1 R_1 \\
r_{CO2} &= \eta_1 R_1 + \eta_3 R_3 + \eta_4 R_4 \\
r_{H2O} &= 2\eta_1 R_1 - \eta_2 R_2 - \eta_3 R_3 - 2\eta_4 R_4 \\
r_{CO} &= \eta_2 R_2 - \eta_3 R_3 \\
r_{H2} &= 3\eta_2 R_2 + \eta_3 R_3 + 4\eta_4 R_4
\end{aligned} \tag{28}$$

Table 4
Adsorption constants

Species	Eq. no.	K_{oi} (/bar)	ΔH^i (kJ/kmol)
O_2	23	5.08×10^4 ($bar^{0.5}$)	66,200
CH_4	23	4.02×10^5	103,500
H_2	27	6.12×10^{-9}	-82,900
CH_4	27	6.65×10^{-4}	-38,280
H_2O	27	1.77×10^5 bar	88,680
CO	27	8.23×10^{-5}	-70,650

Solution Approach To solve the non-linear and coupled governing equations, a CFD code is developed based on the finite volume using the SIMPLE algorithm for the coupling of pressure and velocity domains [Patankar SV. 1980]. The power-law scheme is used for the linearization of the convective terms, and a central difference scheme is employed to linearize the diffusive terms [Hirsch C. 2007]. The algebraic system of equations is then solved using the Jacobian point-to-point iteration method, except for the pressure correction equation, which is solved by exploitation of the Gauss-Seidel iteration method [Versteeg, Malalaskerea 1995].
To save computational time, first the governing equations are solved without considering reactions and property changes. After a number of iterations, this solution is used as an initial guess for the reactive flow calculations.

RESULTS AND DISCUSSION

The present model has been developed for methane ATR in a surface microreactor (as opposed to a packed-bed reactor with volumetric reactions); as a result, there has been difficulty in acquiring compatible data, either experimental or numerical, for its direct validation. In order to qualitatively validate the present work, the experimental results reported by Dias and Assaf [2004] were considered here. The general trends are very similar, but the simulated surface reactor shows lower conversion compared with the actual packed-bed reactor. This was obviously expected, since the two reactors have similar dimensions and operating conditions but the packed-bed reactor had more reaction sites available. Nonetheless, it is observed in both sets of results that increasing temperature leads to an increase in both the H_2 and CO production. This qualitative validation of the simulation results from the present CFD code, gives us confidence in the accuracy of the developed model
In the present study, the effects of three parameters are studied on the performance a methane ATR micro-reactor. Fig. 1 shows the variations of H_2 mole fraction at the reactor outlet and methane conversion for different L/D ratios. The inlet flow conditions for these results are W/F = 3.0, A/F =1.0, and FR = 0.05 m^2/h, and the channel width is 340 μm in all cases.

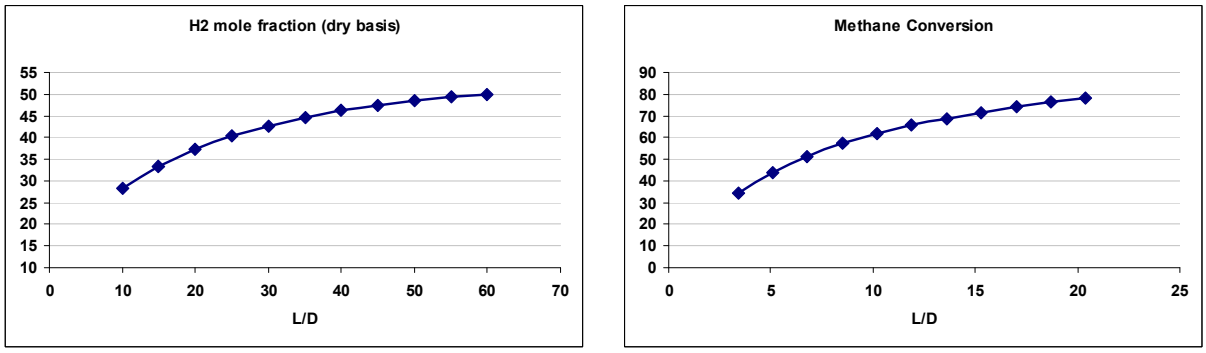

(a) (b)

Figure 1. Variations of (a) H_2 mole fraction, (b) methane conversion, versus channel L/D

It is seen in Fig. 1 that the hydrogen yield increases as the length of the reactor is increased. The reason is that by increasing the reactor length the catalytic surface area of the reactor –where the reactions occur– will increase. The maximum hydrogen yield is obtained for an L/D = 60 at 50% (dry basis). In addition, CO mole fraction for these conditions is 6%, which is small enough to be used in a PEMFC after a further treatments.

In Fig. 2 variations of hydrogen yield and methane conversion versus channel width are shown for a fixed reactor length of 8.5 *mm*. Similar to the first case, the inlet conditions are W/F = 3.0, A/F =1.0, and FR = 0.05 m^2/h.

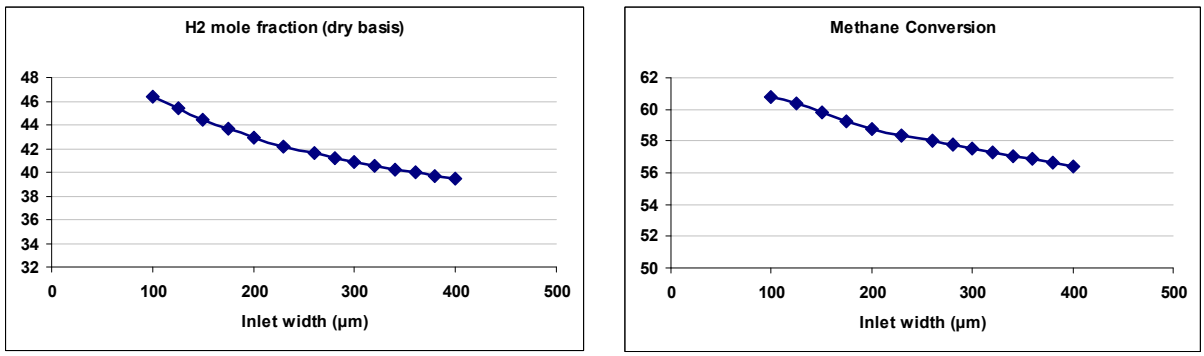

(a) (b)

Figure 2. Variations of (a) H_2 mole fraction, (b) methane conversion, versus channel width

When the channel width is increased at a fixed inlet flow rate, the flux of the inlet mixture will reduce. Thus, diffusion of the reacting species to the walls is also reduced. It is therefore expected that the reaction rates will decrease, resulting in lower methane conversion and hydrogen yield.

Next, the geometry of the reactor is considered to be fixed and effects of the inlet flow rate (FR) are investigated. Fig. 3 represents the results for these cases.

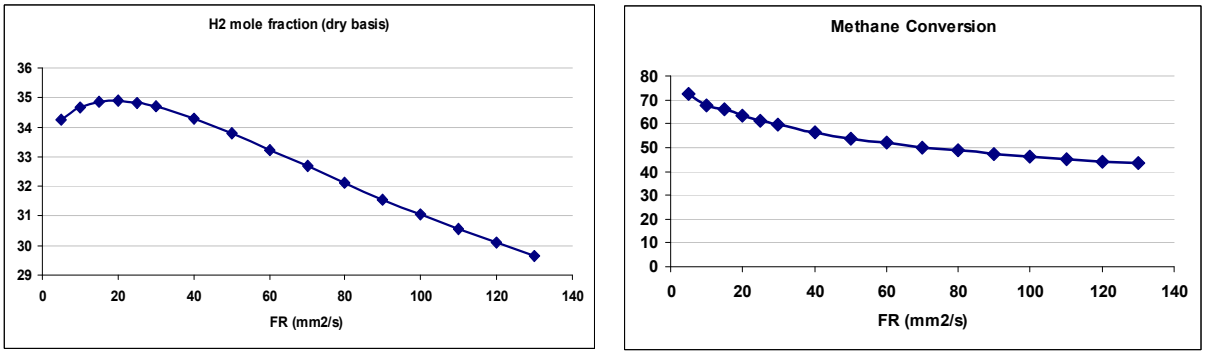

(a) (b)

Figure 3. Variations of (a) H_2 mole fraction, (b) methane conversion, versus inlet flow rate

The inlet mixture composition for this case is W/F = 3.0 and A/F =1.0, and the channel width and length are 340 μm, 8.5 mm, respectively. Results for these cases show that for an inlet flow rate of 20 mm^2/s, the outlet hydrogen mole fraction reaches its maximum value of 34.9% (dry basis). When the flow rate is too low, diffusion phenomenon is controlling the species production rate. By increasing the inlet flow rate up to a specific value, convection of the species will help better transport of the reactants to the wall to produce more hydrogen. However, for higher flow rates, convection of the species will be the controlling parameter and the lower residence time for the species in the reactor will limit hydrogen production.

CONCLUSION

In this study, a two-dimensional, steady state, adiabatic, ATR microreactor for hydrogen production is simulated and effects of three parameters on the hydrogen production are investigated. Results from this work show that by increasing the reactor length the hydrogen yield will increase (up to a limit), while increasing the channel width will decrease the hydrogen production. It is also observed that the inlet flow rate has a significant role in the hydrogen yield. For a fixed geometry of the reactor, the hydrogen yield peaks at a certain flow rate.
Results from this study can be used as a guideline for the design and optimum operation of micro- and mini-channel reactors based on ATR for hydrogen production from methane.

REFERENCES

Ahmed, S., and Krumpelt, M. [2001], Hydrogen from hydrocarbon fuels for fuel cells, *International Journal of Hydrogen Energy*, Vol. 26, pp. 291-301.

de Groote, A.M., and Froment, G.F. [1996], Simulation of the catalytic partial oxidation of methane to synthesis gas, *Applied Catalyst A:General,* Vol. 138, pp. 245-264.

Dias, J.A.C., and Assaf, J.M. [2004], Autothermal reforming of methane over Ni/γ-Al_2O_3 catalysts: the enhancement effect of small quantities of noble metals, *Journal of Power Sources,* Vol. 130, pp. 106-110.

Halabi, M.H., de Croon, M.H.J.M., der Schaaf, J.V., Cobden, P.D., and Schouten, J.C. [2008], Modeling and analysis of autothermal reforming of methane to hydrogen in a fixed bed reformer, *Chemical Engineering Journal,* Vol. 137, pp. 568-578.

Hirsch, C. [2007], *Numerical Computational of Internal and External Flows*, Wiley, Burlington.

Hoang, D.L., and Chan, S.H. [2004], Modeling of a catalytic autothermal methane reformer for fuel cell applications, *Applied Catalyst A:General*, Vol. 268, pp. 207-216.

Larminie, J., and Dicks, A. [2003], *Fuel Cell Systems Explained,* 2nd edition, John Wiley & Sons Ltd., The Atrium, England.

Ma, L., Trimm, D.L., and Jiang, C. [1996], The design and testing of an autothermal reactor for the conversion of light hydrocarbons to hydrogen–I: the kinetics of the catalytic oxidation of light hydrocarbons, *Applied Catalyst A: General*, Vol. 138, pp. 275-283.

Patankar, S.V. [1980], *Numerical heat and fluid flow*, Hemisphere Publ. Co., New York.

Reid, R.C., Prausnitz, J.M., and Poling, B.E. [1987], *The properties of gases and liquids*, McGraw-Hill, New York.

Shukri, M.I., Songip, A.R., Ahmad, A., and Nasri, N.S. [2004], Simulation study of methane autothermal reforming for hydrogen production, *Advances in Fuel Cell Research and Development in Malaysia*, pp. 149-158.

Trimm, D.L., and Lam, C. [1980], The combustion of methane on Platinum-Alumina fibre catalysis–I: kinetics and mechanism, *Chemical Engineering Science*, Vol. 35, pp. 1405-1413.

Versteeg, H.K., and Malalaskerea, W. [1995], *An introduction to computational fluid dynamics: the finite volume method*, Longman, New York.

Xu, J., and Froment, G.F. [1989], Methane steam reforming, methanation and water-gas shift: I. intrinsic kinetics, *AIChE Journal,* Vol. 35, pp. 88-96.